AAAS
Energy Material Advances
Volume 2021, Article ID 2414286, 8 pages
https://doi.org/10.34133/2021/2414286

Energy Material Advances
A SCIENCE PARTNER JOURNAL

Research Article

Rare-Earth Nd Inducing Record-High Thermoelectric Performance of $(GeTe)_{85}(AgSbTe_2)_{15}$

Wan Yu Lyu,[1,2] **Min Hong**,[1,2] **Wei Di Liu**,[1,2] **Meng Li**,[2] **Qiang Sun**,[2] **Sheng Duo Xu**,[2] **Jin Zou**,[2,3] **and Zhi-Gang Chen**[1,2]

[1]*Centre for Future Materials, University of Southern Queensland, Springfield, Queensland 4300, Australia*
[2]*School of Mechanical and Mining Engineering, The University of Queensland, Brisbane, Queensland 4072, Australia*
[3]*Centre for Microscopy and Microanalysis, The University of Queensland, Brisbane, Queensland 4072, Australia*

Correspondence should be addressed to Zhi-Gang Chen; zhigang.chen@usq.edu.au

Received 5 December 2020; Accepted 19 January 2021; Published 16 March 2021

As a promising midtemperature thermoelectric material with both higher thermoelectric performance and mechanical property, Tellurium Antimony Germanium Silver (TAGS-*x*), written as $(GeTe)_x(AgSbTe_2)_{1-x}$, especially $(GeTe)_{0.85}(AgSbTe_2)_{0.15}$ (TAGS-85), has attracted wide attention. Herein, we innovatively use Nd doping to synergistically decrease the carrier concentration to the optimal level leading to enhanced dimensionless figure of merit, zT. Our density-functional theory calculation results indicate that Nd-doping reduced carrier concentration should be attributed to the enlargement of band gap. The optimized carrier concentration results in an ultrahigh power factor of ~32 $\mu W\,cm^{-1}\,K^{-2}$ at 727 K in $Ge_{0.74}Ag_{0.13}Sb_{0.11}Nd_{0.02}Te$. Simultaneously, the lattice thermal conductivity of $Ge_{0.74}Ag_{0.13}Sb_{0.11}Nd_{0.02}Te$ retained as low as ~0.5 at 727 K. Ultimately, a record-high zT of 1.65 at 727 K is observed in the $Ge_{0.74}Ag_{0.13}Sb_{0.11}Nd_{0.02}Te$. This study indicates rare-earth Nd doping is effective in boosting the thermoelectric performance of TAGS-85 and approached a record-high level via synergistic effect.

1. Introduction

Fossil fuel overexploitation and the corresponding environment pollution have called for growing development of sustainable energy-utilization technologies [1]. Thermoelectrics, which can achieve the reciprocal energy conversion between heat and electricity, are one promising candidate [2, 3]. However, the wide commercialization of thermoelectrics is limited by the low thermoelectric energy conversion efficiency, evaluated by the dimensionless figure of merit, $zT = S^2\sigma T/\kappa_{total}$. Here, S is the Seebeck coefficient, σ is the electrical conductivity, and κ_{total} represents the total thermal conductivity (accumulation of electron (κ_e) and lattice (κ_l) parts) [4]. $S^2\sigma$ is defined as the power factor to evaluate the overall electrical performance. To enhance zT, both high $S^2\sigma$ and low κ_{total} are required. Multiple strategies have been developed to enhance $S^2\sigma$ of thermoelectric materials, such as carrier concentration (n, n_p for holes) optimization [5, 6], resonance level engineering [7], band convergence [8–10], energy filtering [11], quantum confinement [12], and Rashba effect [13]. Alternatively, hierarchical phonon scattering centers, including point defects, dislocations, stacking faults, dense grain boundaries [14, 15], and phase interfaces, can effectively decrease κ_l and κ_{total} to achieve high zT values [16, 17].

IV-VI tellurides (Ge/Sn/Pb-Te) are promising midtemperature thermoelectric materials due to their relatively high zT values [5, 18–21]. For example, PbTe-based thermoelectric material has approached the high zT value of 2.2 at 915 K in PbTe-4 mol.% SrTe with 2 mol.% Na [18, 22]. However, the high toxicity of Pb limits its practical application. Alternatively, κ_l of SnTe is relatively higher which leads to lower zT value of only 1.51 at 800 K [23] comparing with PbTe [18] and GeTe [24]. Therefore, nontoxic and high-performance GeTe-based thermoelectric materials, with the peak zT values higher than 2 [24, 25], have attracted extensive attention. To boost the thermoelectric performance of GeTe with good mechanical property and make it suitable for application, rhombohedral GeTe is alloyed with cubic $AgSbTe_2$ and forms a continuous solid solution, called as Tellurium Antimony Germanium Silver (TAGS-*x*,

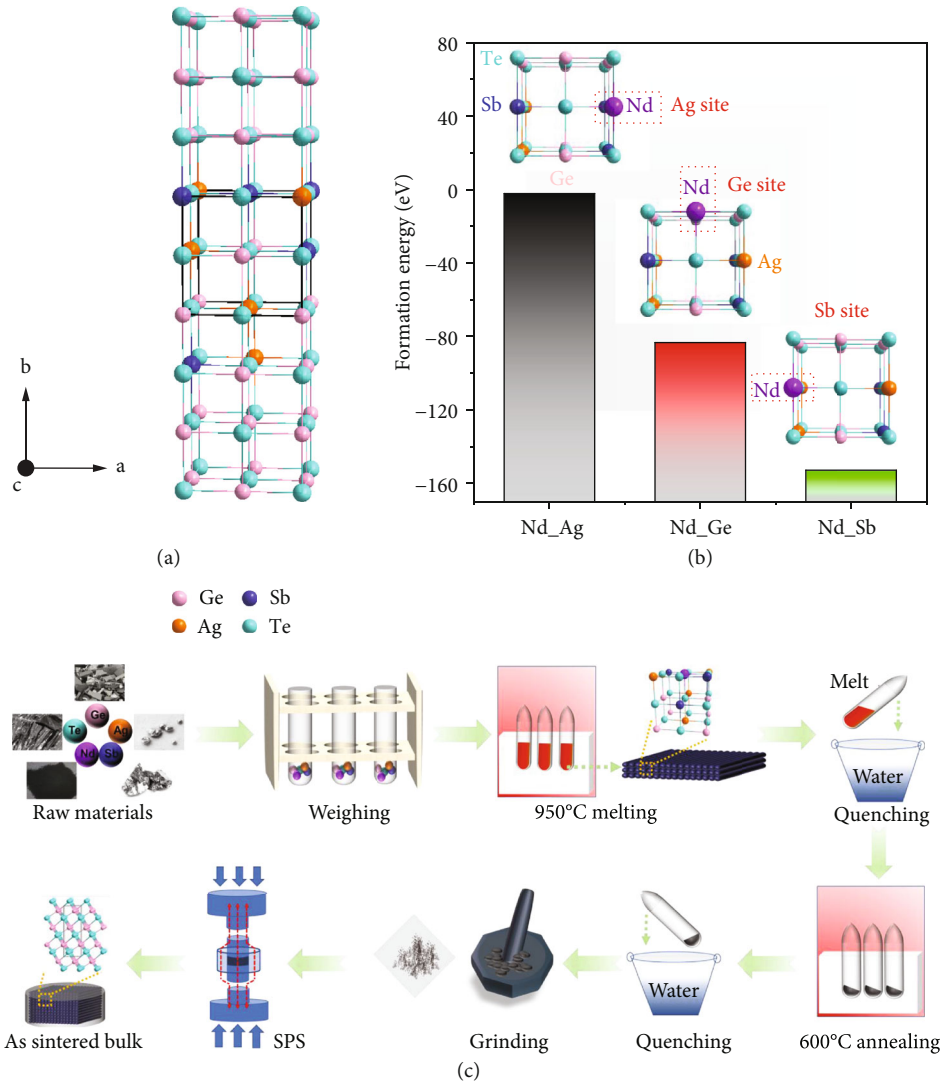

FIGURE 1: Experimental design and synthesis process. (a) Crystal structure of cubic TAGS-85; (b) calculated formation energy for Nd doping in Ag, Ge, and Sb sites of cubic TAGS-85, respectively; (c) schematic diagram of the experiment preparation process.

written as $(GeTe)_x(AgSbTe_2)_{1-x}$, where x ranges from 0.7 to 0.9) [26, 27]. TAGS-85, which can also be written as $Ge_{0.74}Ag_{0.13}Sb_{0.13}Te$, has approached the highest peak zT (zT_{max}) of 1.36 at 700 K with good mechanical properties (elastic modulus of 50 GPa and Poisson's ratio of 0.24) [27]. However, the thermoelectric performance of TAGS-85 is still lower than other state-of-the-art thermoelectric materials, such as PbTe [28]. Thus, recent studies of TAGS-85 focus on further improving the thermoelectric performance. Self-doping achieved by tuning the ratio of Ag/Sb ratio can effectively enhance the zT_{max} value of TAGS-85 up to 1.6 at 750 K [29]. Levin et al. [30, 31] reported that the large atomic size and localized magnetic moment of rare-earth elements Dy, Yb, and Ce can increase zT values of TAGS-85. For example, 1% Ce and 1% Yb substitution in Te site can boost up S by 16% to 205 $\mu V\,K^{-1}$ [30], attributed to the localized paramagnetic moment, leading to an enhanced zT_{max} of 1.5 at 700 K.

To better understand the influence of rare-earth element doping on thermoelectric performance of TAGS-85, we selected Nd as the dopant to optimize thermoelectric performance of TAGS-85. As a rare-earth element, Nd as dopant can affect transport properties of thermoelectric materials in many ways: (a) Nd doping in TAGS-85 can result in local lattice distortion due to larger atomic size; (b) multielectron Nd^{3+} can affect carrier concentration due to different valence electron counts or influence of the chemical bond [32]; (c) different with large localized magnetic moments of Ce ($4f^15d^16s^2$) and Yb ($4f^{13}6s^2$), Nd ($4f^46s^2$) has small localized magnetic effect, which can induce interesting change to S [30, 31]. Considering the complex crystal structure of TAGS-85, three cation sites (Ge, Ag, and Sb) can be substitute by Nd (Figure 1(a)). Figure 1(b) compares the formation energy of Nd substitution at different cation sites of TAGS-85. As can be seen, Nd can preferentially substitute Sb due to the lowest formation energy. Here, we design the sample with nominal composition as $Ge_{0.74}Ag_{0.13}Sb_{0.13-x}Nd_xTe$ ($x = 0$, 0.02, and 0.04). Figure 1(c) schematically shows the experiment process, where all samples are prepared by

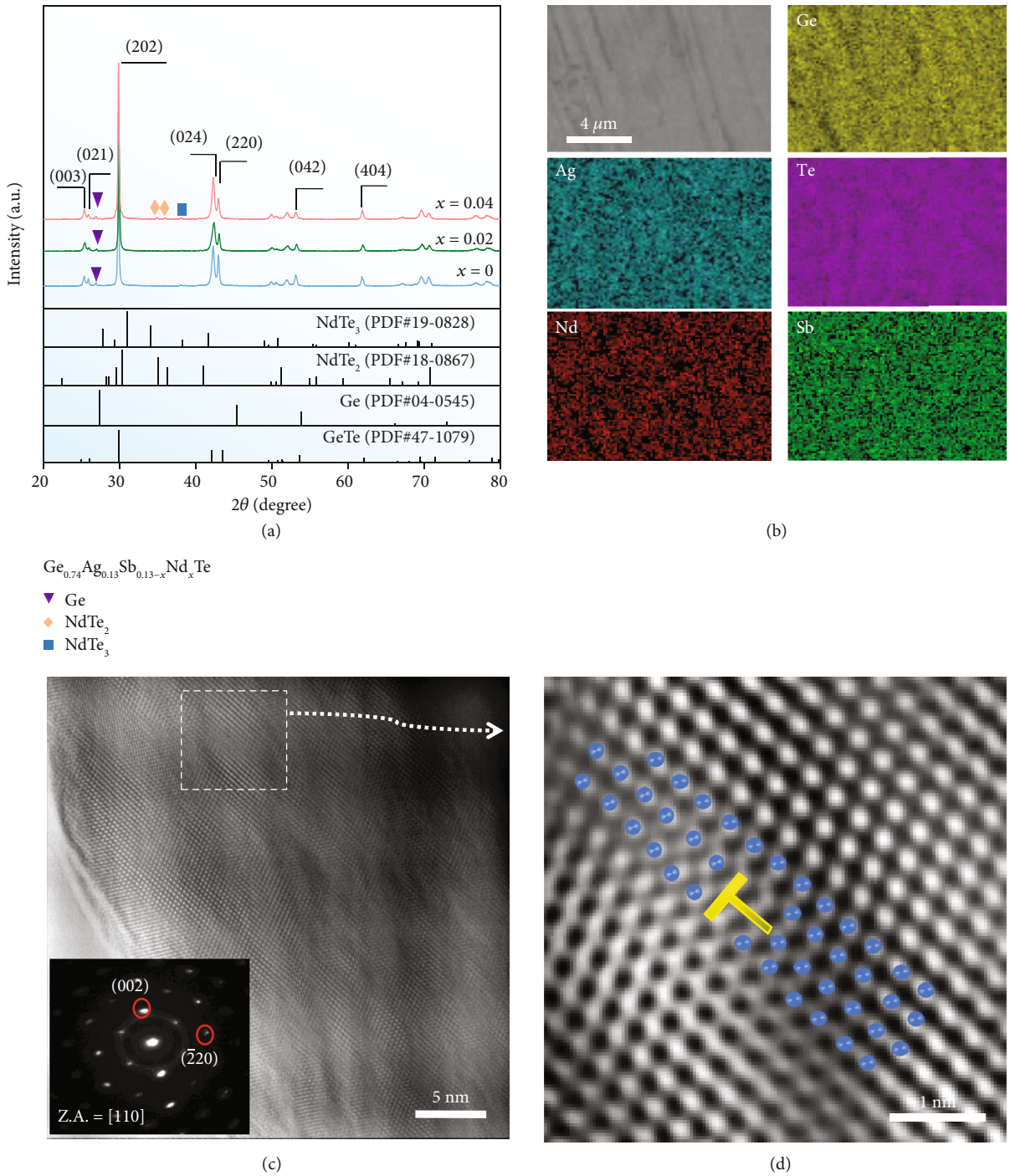

Figure 2: Characterization of crystal structure and microstructure morphologies. (a) XRD patterns of as-sintered $Ge_{0.74}Ag_{0.13}Sb_{0.13-x}Nd_xTe$ ($x = 0$, 0.02, and 0.04) pellets, (b) backscattered SEM images of corresponding EDS element maps of as-sintered $Ge_{0.74}Ag_{0.13}Sb_{0.11}Nd_{0.02}Te$ pellet, (c) HRTEM image of as-sintered $Ge_{0.74}Ag_{0.13}Sb_{0.11}Nd_{0.02}Te$ pellet (inset is the corresponding SAED pattern in [110] zone axis (Z.A.)), and (d) enlarged HRTEM of white square circled area in (c).

melting, quenching, annealing, and spark plasma sintering (SPS). Our results show that Nd doping can effectively reduce n_p of TAGS-85 close to the optimal level due to band gap enlargement. Correspondingly, zT_{max} can be boosted to as high as 1.65 in $Ge_{0.74}Ag_{0.13}Sb_{0.11}Nd_{0.02}Te$.

2. Experimental Methods

2.1. Synthesis. Polycrystalline Nd-doped TAGS-85 was prepared in the formulae of $Ge_{0.74}Ag_{0.13}Sb_{0.13-x}Nd_xTe$ ($x = 0$, 0.02, and 0.04). Precursors, including Ge (99.999%, Sigma-

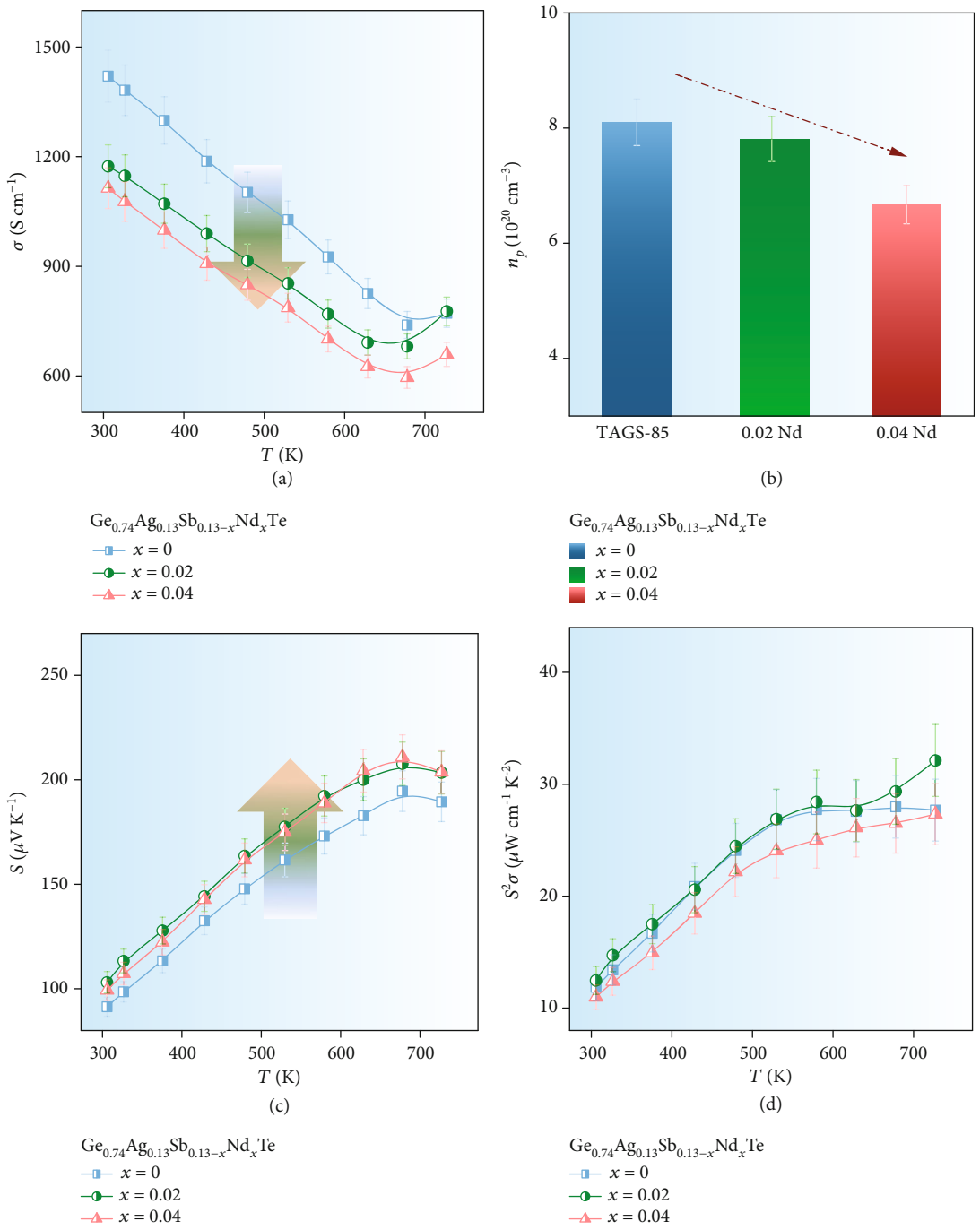

Figure 3: Electrical property of the as-sintered $Ge_{0.74}Ag_{0.13}Sb_{0.13-x}Nd_xTe$ ($x = 0$, 0.02, and 0.04) pellets. (a) Temperature-dependent σ, (b) room temperature n_p, (c) temperature-dependent S, and (d) $S^2\sigma$ of the as-sintered $Ge_{0.74}Ag_{0.13}Sb_{0.13-x}Nd_xTe$ ($x = 0$, 0.02, and 0.04) pellets.

Aldrich, Australia), Te (99.999%, Sigma-Aldrich, Australia), Ag (99.99%, Sigma-Aldrich, United States), Sb (99.999%, Alfa Aesar, United States), and Nd (99.999%, Alfa Aesar, United States), were weighed following the nominal compositions. The weighted precursors were sealed in quartz ampules and heated in 1223 K for 12 hours followed by water quenching. The obtained samples were further annealed at 873 K for 2 days and quenched again. This two-step quenching method is designed to reduce Ge vacancies and inhibit the formation of the second phase, Ag_8GeTe_6 [33]. The resultant products were further ground into powders and sintered into pellets (SPS, 65 MPa and 673 K) for performance measurement.

2.2. Characterization. The crystal structures of as-prepared samples were characterized by X-ray diffraction (XRD, Bruker, United States, Cu K_α radiation with a wavelength of 1.5418 Å, $10° \le 2\theta \le 80°$, step with 0.02°). A field-emission scanning electron microscope (FE-SEM, JSM-7001F, JEOL, Japan) equipped with energy-dispersive spectrum (EDS)

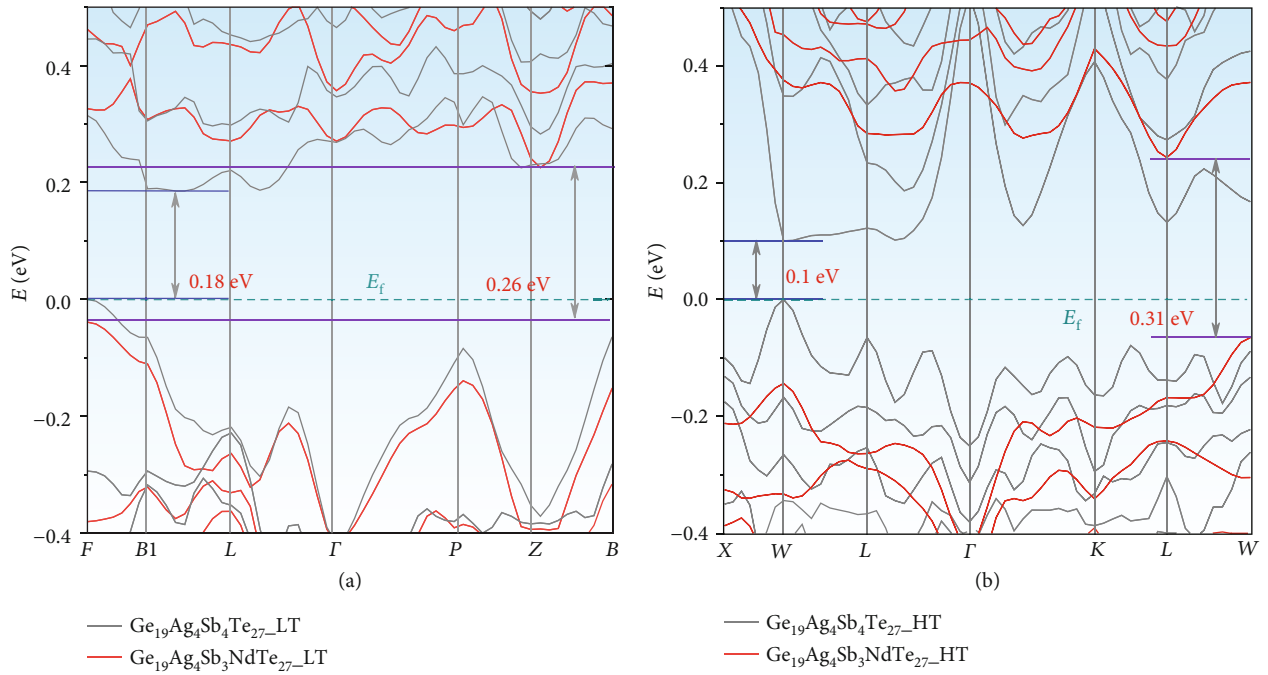

FIGURE 4: Calculated band structures of pristine TAGS-85 ($Ge_{19}Ag_4Sb_4Te_{27}$) and Nd-doped TAGS-85 ($Ge_{19}Ag_4Sb_3Nd_1Te_{27}$) in (a) low-temperature phase and (b) high-temperature phase.

detector was employed to explore the morphologies and compositions. To further understand the structural information, the $Ge_{0.74}Ag_{0.13}Sb_{0.11}Nd_{0.02}Te$ sample was characterized by a transmission electron microscope (TEM, Tecnai F20, Philips, United States).

2.3. Thermoelectric Property Measurement. S and σ of the sintered pellets were simultaneously measured by ZEM-3 (ULVAC Technologies, Inc., Japan). κ_{total} is calculated by $\kappa_{total} = D \times C_p \times \rho$, where C_p is the specific heat estimated from the Dulong-Petit approximation [34], ρ is the pellet densities measured by Archimedes method, the densities are shown in supporting information Table S1, and D is the thermal diffusivity coefficient measured by the laser flash diffusivity apparatus (LFA 457, Netzsch, Germany). The Hall coefficient (R_H) was measured based on the Van der Pauw technique [35]. n_p and hole mobility (μ) were through the equation $n_p = 1/(eR_H)$ and $\mu = \sigma R_H$, where e is the electron charge.

2.4. Density Functional Theory Calculations. Band structures were calculated by using the plane-wave self-consistent field code [36]. A uniform mesh of $2 \times 2 \times 2k$-points was used in sampling integrations over the Brillouin zone. The band structures of pristine TAGS-85 and Nd-doped TAGS-85 were calculated based on $Ge_{19}Ag_4Sb_4Te_{27}$ and $Ge_{19}Ag_4Sb_3Nd_1Te_{27}$ with the uniform mesh of $2 \times 2 \times 2k$-points, respectively.

3. Results and Discussions

Figure 2(a) shows room temperature X-ray diffraction (XRD) patterns of the as-sintered ($Ge_{0.74}Ag_{0.13}Sb_{0.13-x}Nd_xTe$) ($x = 0$, 0.02, and 0.04) pellets. All main peaks can be indexed as R-GeTe (space group R3m) whose structure is a slightly distorted rock-salt structure along the [111] direction [20]. Ge precipitates (purple triangle) were detected as normal due to the nature of easily formed Ge vacancies in GeTe-based thermoelectric materials [37–39]. When the Nd doping level reaches as high as $x = 0.04$, $NdTe_2$ (yellow diamond) and $NdTe_3$ (blue square) impurities can be found. Figure 2(b) shows the backscattered scanning electron microscopy (SEM) image and corresponding energy-dispersive spectrum (EDS) maps of the $Ge_{0.74}Ag_{0.13}Sb_{0.11}Nd_{0.02}Te$ sample. As can be seen, Ge, Te, Ag, Sb, and Nd are homogeneously distributed in the matrix, indicating that Nd has successfully doped into TAGS-85. Figures 2(c) and 2(d) show high-resolution (HR) transition electron microscopy (TEM) image of $Ge_{0.74}Ag_{0.13}Sb_{0.11}Nd_{0.02}Te$ pellet along the [110] zone axis (indexed from the selected area electron diffraction (SEAD) pattern as shown in the inset of Figure 2(c)). Figure 2(d) shows its enlarged HRTEM image in the marked square area of Figure 2(c), where the dislocations caused by Nd doping-induced dense point defects can be clearly observed.

Figure 3(a) shows temperature-dependent σ of the as-sintered $Ge_{0.74}Ag_{0.13}Sb_{0.13-x}Nd_xTe$ pellets. All samples show degenerated semiconducting behavior, and σ of $Ge_{0.74}Ag_{0.13}Sb_{0.11}Nd_{0.02}Te$ decreases from 1178.10 at room temperature to 687.45 S cm^{-1} at 673 K. With increasing the Nd doping level, σ at room temperature reduces from 1424.45 to 1108.89 S cm^{-1}. The observed reduced σ should be attributed to reduced n_p as shown in Figure 3(b). Figure 3(c) shows temperature-dependent S of the as-sintered $Ge_{0.74}Ag_{0.13}Sb_{0.13-x}Nd_xTe$ pellets. With increasing the Nd doping level, room temperature S of $Ge_{0.74}Ag_{0.13}Sb_{0.13-x}Nd_xTe$ slightly increases from 92 to 104 μV K^{-1} due to the reduced n_p. S of $Ge_{0.74}Ag_{0.13}Sb_{0.09}Nd_{0.04}Te$ can approach as high as 210 μV K^{-1} at 678 K.

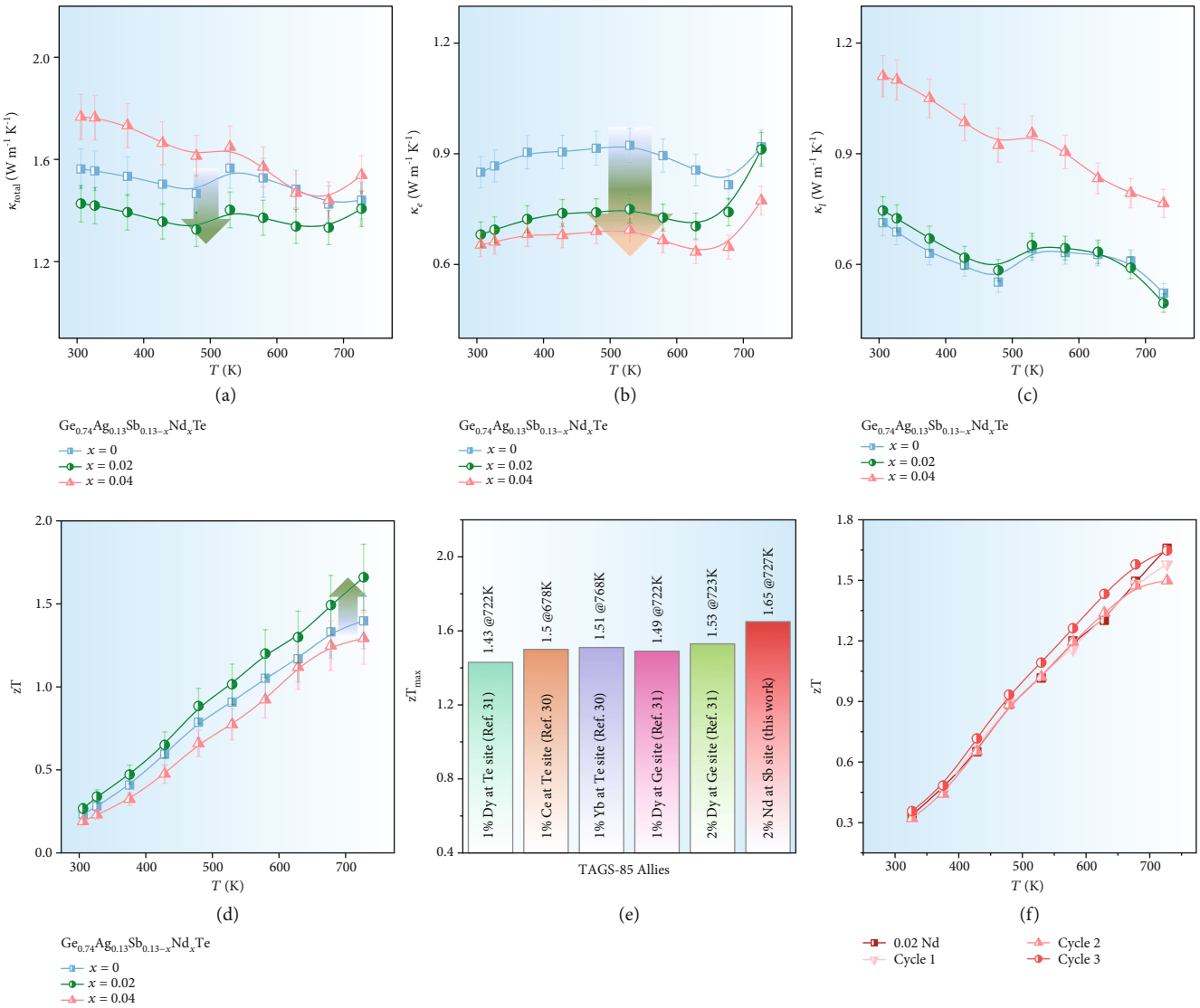

FIGURE 5: Analysis of thermal performance and optimized zT values. (a) Temperature-dependent κ_{total}, (b) κ_e, (c) κ_l, and (d) zT values of the as-sintered $Ge_{0.74}Ag_{0.13}Sb_{0.13-x}Nd_xTe$ ($x = 0$, 0.02, and 0.04). (e) Comparison of the obtained zT_{max} of $Ge_{0.74}Ag_{0.13}Sb_{0.11}Nd_{0.02}Te$ with other rare-earth element-doped TAGS-85 [30, 31] and (f) cycle test results for $Ge_{0.74}Ag_{0.13}Sb_{0.11}Nd_{0.02}Te$.

Figure 3(d) illustrates temperature-dependent $S^2\sigma$ of the as-sintered $Ge_{0.74}Ag_{0.13}Sb_{0.13-x}Nd_xTe$ pellets. An enhanced $S^2\sigma$ of 32 μW cm^{-1} K^{-2} at 727 K can be observed in $Ge_{0.74}Ag_{0.13}Sb_{0.11}Nd_{0.02}Te$.

To understand the change of electrical transport properties, we calculated the electronic band structure of pristine TAGS-85 ($Ge_{19}Ag_4Sb_4Te_{27}$) and Nd-doped TAGS-85 ($Ge_{19}Ag_4Sb_3Nd_1Te_{27}$). Figure 4(a) compares the calculated electronic band structures of low-temperature (LT) $Ge_{19}Ag_4Sb_4Te_{27}$ and $Ge_{19}Ag_4Sb_3Nd_1Te_{27}$. After Nd doping, the valence band maximum (VBM) shifts result in changed band gap from indirect to direct type. The band gap increases from 0.18 eV of $Ge_{19}Ag_4Sb_4Te_{27}$ to 0.26 eV of $Ge_{19}Ag_4Sb_3Nd_1Te_{27}$. Nd doping also effectively enlarges the band gap of high-temperature (HT) TAGS-85 from 0.1 eV of $Ge_{19}Ag_4Sb_4Te_{27}$ to 0.31 eV of $Ge_{19}Ag_4Sb_3Nd_1Te_{27}$, as shown in Figure 4(b). The enlarged band gap of both LT and HT TAGS-85 after Nd doping can well explain the decrease of n_p.

Figures 5(a)–5(c) show temperature-dependent thermal transport properties of the as-sintered $Ge_{0.74}Ag_{0.13}Sb_{0.13-x}Nd_xTe$ pellets. As shown in Figure 5(a), κ_{total} of TAGS-85 slightly decreases after Nd doping. However, with increasing the content of Nd to 0.04, the room temperature κ_{total} increases to 1.76 W m^{-1} K^{-1}. To better understand the effect of Nd doping on the thermal transport properties of TAGS-85, κ_e and κ_l were further calculated as shown in Figures 5(b) and 5(c). κ_l was estimated by subtracting κ_e from κ_{total}. κ_e and the Lorenz number (L) were calculated based on the classic single parabolic band model. As can be seen, κ_e decreases from 0.85 to 0.65 W m^{-1} K^{-1} at room temperature with increasing the Nd content due to reduced σ. With 2% Nd doping, κ_l shows no obvious change. When the Nd doping level further increases to 4% to surpass the solubility limit, the room temperature κ_l increases from 0.70 to 1.11 W m^{-1} K^{-1} due to additional impurity phases $NdTe_2$ and $NdTe_3$ [40]. Figure 5(d) plots temperature-dependent

zT values of the as-sintered $Ge_{0.74}Ag_{0.13}Sb_{0.13-x}Nd_xTe$ pellets and shows increased zT values with increasing temperature. The zT_{max} value of $Ge_{0.74}Ag_{0.13}Sb_{0.11}Nd_{0.02}Te$ can reach 1.65 at 727 K. Figure 5(e) compares the zT_{max} values of this study with previously reported Ce-, Yb-, and Dy-doped TAGS-85 [30, 31]. In our study, Nd tends to substitute the Sb site, which is different from Ce, Yb (Te site), and Dy (Ge site). Different occupation sites can result in various effects on electrical and thermal properties. Thus, Nd doping in the Sb site can decrease both the carrier concentration and thermal conductivity. This results in the highest zT value of 1.65 at 727 K. Figure 5(f) presents the reproductivity of $Ge_{0.74}Ag_{0.13}Sb_{0.11}Nd_{0.02}Te$ in three cycling tests, suggesting high stability of the Nd-doped TAGS-85.

4. Conclusion

In this study, we achieve a record-high zT of 1.65 at 727 K in $Ge_{0.74}Ag_{0.13}Sb_{0.11}Nd_{0.02}Te$ mainly due to κ_{total} reduction while maintaining high $S^2\sigma$. Reduced κ_{total} should be attributed to reduced σ due to decreased n_p. Although reduced n_p deteriorates σ, reduced n_p also slightly increases S, leading to nearly unchanged $S^2\sigma$. Our DFT calculation suggests that reduced n_p is caused by the Nd doping-induced band gap enlargement. Comparing with other rare-earth elements, Nd is more effective in enhancing the thermoelectric performance of TAGS-85. The Nd-doped TAGS-85 also shows high stability.

Data Availability

All data required to support this study are presented in the paper and the supporting document. Additional data are available upon request from the authors.

Conflicts of Interest

The authors declare that they have no conflicts of interest.

Acknowledgments

This work was financially supported by the Australian Research Council, Innovation Centre for Sustainable Steel project, and University of Southern Queensland strategic research grant. LWY thanks the Chinese Scholarship Council for providing the Ph.D. stipend.

Supplementary Materials

Figure S1: Hall mobility (μ) of the Nd-doped TAGS-85 at the room temperature. Table S1: the density of as-prepared samples. *(Supplementary Materials)*

References

[1] J. He and T. M. Tritt, "Advances in thermoelectric materials research: looking back and moving forward," *Science*, vol. 357, no. 6358, article eaak9997, 2017.

[2] G. J. Snyder and E. S. Toberer, "Complex thermoelectric materials," *Nature Materials*, vol. 7, no. 2, pp. 105–114, 2008.

[3] L. E. Bell, "Cooling, heating, generating power, and recovering waste heat with thermoelectric systems," *Science*, vol. 321, no. 5895, pp. 1457–1461, 2008.

[4] D. M. Rowe, *Thermoelectrics-Handbook-Macro-to-Nano*, CRC Press, 2006.

[5] Y. Pei, A. D. LaLonde, N. A. Heinz et al., "Stabilizing the optimal carrier concentration for high thermoelectric efficiency," *Advanced Materials*, vol. 23, no. 47, pp. 5674–5678, 2011.

[6] Y. Pei, A. F. May, and G. J. Snyder, "Self-tuning the carrier concentration of PbTe/Ag2Te composites with excess Ag for high thermoelectric performance," *Advanced Energy Materials*, vol. 1, no. 2, pp. 291–296, 2011.

[7] M. Hong, Z. G. Chen, L. Yang et al., "Realizing *zT* of 2.3 in $Ge_{1-x-y}Sb_xIn_yTe$ via reducing the phase-transition temperature and introducing resonant energy doping," *Advanced Materials*, vol. 30, no. 11, article 1705942, 2018.

[8] Y. Tang, Z. M. Gibbs, L. A. Agapito et al., "Convergence of multi-valley bands as the electronic origin of high thermoelectric performance in $CoSb_3$ skutterudites," *Nature Materials*, vol. 14, no. 12, pp. 1223–1228, 2015.

[9] Y. Pei, H. Wang, and G. J. Snyder, "Band engineering of thermoelectric materials," *Advanced Materials*, vol. 24, no. 46, pp. 6125–6135, 2012.

[10] W. He, D. Wang, H. Wu et al., "High thermoelectric performance in low-cost $SnS_{0.91}Se_{0.09}$ crystals," *Science*, vol. 365, no. 6460, pp. 1418–1424, 2019.

[11] H. R. Yang, J. H. Bahk, T. Day et al., "Enhanced Thermoelectric Properties in Bulk Nanowire Heterostructure-Based Nanocomposites through Minority Carrier Blocking," *Nano Letters*, vol. 15, no. 2, pp. 1349–1355, 2015.

[12] M. S. Dresselhaus, G. Chen, M. Y. Tang et al., "New directions for low-dimensional thermoelectric materials," *Advanced Materials*, vol. 19, no. 8, pp. 1043–1053, 2007.

[13] M. Hong, W. Lyv, M. Li et al., "Rashba Effect Maximizes Thermoelectric Performance of GeTe Derivatives," *Joule*, vol. 4, no. 9, pp. 2030–2043, 2020.

[14] H. Xie, H. Wang, Y. Pei et al., "Beneficial contribution of alloy disorder to electron and phonon transport in half-Heusler thermoelectric materials," *Advanced Functional Materials*, vol. 23, no. 41, pp. 5123–5130, 2013.

[15] J. Mao, J. L. Niedziela, Y. Wang et al., "Self-compensation induced vacancies for significant phonon scattering in InSb," *Nano Energy*, vol. 48, pp. 189–196, 2018.

[16] L. Yang, Z.-G. Chen, G. Han, M. Hong, Y. Zou, and J. Zou, "High-performance thermoelectric Cu_2Se nanoplates through nanostructure engineering," *Nano Energy*, vol. 16, pp. 367–374, 2015.

[17] S. N. Girard, J. He, C. Li et al., "In situ nanostructure generation and evolution within a bulk thermoelectric material to reduce lattice thermal conductivity," *Nano Letters*, vol. 10, no. 8, pp. 2825–2831, 2010.

[18] K. Biswas, J. He, I. D. Blum et al., "High-performance bulk thermoelectrics with all-scale hierarchical architectures," *Nature*, vol. 489, no. 7416, pp. 414–418, 2012.

[19] Q. Zhang, B. Liao, Y. Lan et al., "High thermoelectric performance by resonant dopant indium in nanostructured SnTe," *Proceedings National Academy of Sciences of the United States of America*, vol. 110, no. 33, pp. 13261–13266, 2013.

[20] M. Hong, Y. Wang, W. D. Liu et al., "Arrays of planar vacancies in superior thermoelectric $ge_{1-x-y}Cd_xBi_yTe$ with band

convergence," *Advanced Energy Materials*, vol. 8, no. 30, article 1801837, 2018.

[21] J. Li, Z. W. Chen, X. Y. Zhang, Y. X. Sun, J. Yang, and Y. Z. Pei, "Electronic origin of the high thermoelectric performance of GeTe among the p-type group IV monotellurides," *NPG Asia Materials*, vol. 9, no. 3, article e353, 2017.

[22] Y. J. Kim, L. D. Zhao, M. G. Kanatzidis, and D. N. Seidman, "Analysis of nanoprecipitates in a Na-doped PbTe–SrTe thermoelectric material with a high figure of merit," *ACS Applied Materials & Interfaces*, vol. 9, no. 26, pp. 21791–21797, 2017.

[23] Z. Ma and J. Lei, "Enhancement of thermoelectric properties in Pd–In Co-doped SnTe and its phase transition behavior," *ACS Applied Materials & Interfaces*, vol. 11, no. 37, pp. 33792–33802, 2019.

[24] M. Hong, Y. Wang, T. L. Feng et al., "strong phonon–phonon interactions securing extraordinary thermoelectric $Ge_{1-x}Sb_xTe$ with Zn-alloying-induced band alignment," *Journal of the American Chemical Society*, vol. 141, pp. 1742–1748, 2019.

[25] L. Xie, Y. Chen, R. Liu et al., "Stacking faults modulation for scattering optimization in GeTe-based thermoelectric materials," *Nano Energy*, vol. 68, article 104347, 2020.

[26] J. R. Salvador, J. Yang, X. Shi, H. Wang, and A. A. Wereszczak, "Transport and mechanical property evaluation of $(AgSbTe)_{1-x}(GeTe)_x$(x=0.80, 0.82, 0.85, 0.87, 0.90)," *Journal of Solid State Chemistry*, vol. 182, no. 8, pp. 2088–2095, 2009.

[27] H. S. Kim, P. Dharmaiah, and S. J. Hong, "Thermoelectric properties of texture-controlled $(GeTe)_x(AgSbTe_2)_{100-x}$ (x=75, 80, 85, and 90) alloys fabricated by gas-atomization and hot-extrusion processes," *Journal of Electronic Materials*, vol. 47, no. 6, pp. 3119–3126, 2018.

[28] H. J. Wu, L. D. Zhao, F. S. Zheng et al., "Broad temperature plateau for thermoelectric figure of merit ZT>2 in phase-separated $PbTe_{0.7}S_{0.3}$," *Nature Communications*, vol. 5, no. 1, article 4515, 2014.

[29] T. J. Zhu, H. L. Gao, Y. Chen, and X. B. Zhao, "Ioffe–Regel limit and lattice thermal conductivity reduction of high performance $(AgSbTe_2)_{15}(GeTe)_{85}$ thermoelectric materials," *Journal of Materials Chemistry A*, vol. 2, no. 9, pp. 3251–3256, 2014.

[30] E. M. Levin, B. A. Cook, J. L. Harringa, S. L. Bud'ko, R. Venkatasubramanian, and K. Schmidt-Rohr, "Analysis of Ce- and Yb-doped TAGS-85 materials with enhanced thermoelectric figure of merit," *Advanced Functional Materials*, vol. 21, no. 3, pp. 441–447, 2011.

[31] E. M. Levin, S. L. Bud'ko, and K. Schmidt-Rohr, "Enhancement of thermopower of TAGS-85 high-performance thermoelectric material by doping with the rare earth Dy," *Advanced Functional Materials*, vol. 22, no. 13, pp. 2766–2774, 2012.

[32] A. Novitskii, G. Guélou, D. Moskovskikh et al., "Reactive spark plasma sintering and thermoelectric properties of Nd-substituted BiCuSeO oxyselenides," *Journal of Alloys and Compounds*, vol. 785, pp. 96–104, 2019.

[33] A. Kumar, P. A. Vermeulen, B. J. Kooi et al., "A cubic room temperature polymorph of thermoelectric TAGS-85," *RSC Advances*, vol. 8, no. 74, pp. 42322–42328, 2018.

[34] J. Li, X. Y. Zhang, S. Q. Lin, Z. W. Chen, and Y. Z. Pei, "Realizing the high thermoelectric performance of GeTe by Sb-doping and Se-alloying," *Chemistry of Materials*, vol. 29, no. 2, pp. 605–611, 2017.

[35] K. A. Borup, E. S. Toberer, L. D. Zoltan et al., "123902Measurement of the electrical resistivity and Hall coefficient at high temperatures," *The Review of Scientific Instruments*, vol. 83, no. 12, 2012.

[36] P. Giannozzi, O. Andreussi, T. Brumme et al., "QUANTUM ESPRESSO: a modular and open-source software project for quantum simulations of materials," *Journal of Physics: Condensed Matter*, vol. 21, no. 39, article 395502, 2009.

[37] A. Edwards, A. Pineda, P. Schultz et al., "Electronic structure of intrinsic defects in crystalline germanium telluride," *Physical Review B*, vol. 73, no. 4, article 045210, 2006.

[38] D. H. Damon, M. S. Lubell, and R. Mazelsky, "Nature of the defects in germanium telluride," *Journal of Physics and Chemistry of Solids*, vol. 28, no. 3, pp. 520–522, 1967.

[39] F. Fahrnbauer, D. Souchay, G. Wagner, and O. Oeckler, "High thermoelectric figure of merit values of germanium antimony tellurides with kinetically stable cobalt germanide precipitates," *Journal of the American Chemical Society*, vol. 137, no. 39, pp. 12633–12638, 2015.

[40] S. Kim and H. S. Lee, "Effects of addition of Si and Sb on the microstructure and thermoelectric properties of GeTe," *Metals and Materials International*, vol. 25, no. 2, pp. 528–538, 2019.